SAPHARI

Safe and Autonomous Physical Human-Aware Robot Interaction

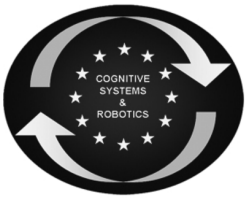

Project funded by the European Community's 7th Framework Programme (FP7-ICT-2011-7)
Grant Agreement ICT–287513

Deliverable D3.4.1

Intentional human-interaction control of compliant robots

Deliverable due date: 30 April 2015	**Actual submission date:** 15 July 2015
Start date of project: 1 November 2011	**Duration:** 48 months
Lead beneficiary: UNIROMA1	**Revision:** Final

Nature: R	**Dissemination level:** PU
R = Report P = Prototype D = Demonstrator O = Other	PU = Public PP = Restricted to other programme participants (including the Commission Services) RE = Restricted to a group specified by the consortium (including the Commission Services) CO = Confidential, only for members of the consortium (including the Commission Services)

Executive Summary

This is the seond to last deliverable of work package WP3, presenting the results on intentional human-robot interaction (HRI) obtained by the partners of SAPHARI. In this document, control strategies are reported for robots with compliant joints or Variable Stiffness Actuation (VSA) that allow safe and effective intentional HRI. These approaches are the most recent tools developed within task T3.4 “Interaction control” of SAPHARI. The methods add new skills for redundant robots that complete the set of capabilities illustrated in a series of previous reports, and in particular: D3.3.1 “Safe dynamic control laws for redundant robots”, MS3 “Optimal control of modular VSA manipulators”, MS11 “Safe kinematic control laws for redundant robots”, MS12 “Force control laws for VIA manipulators”, and MS29 “Impedance control laws for VIA manipulators”.

Table of contents

1 Introduction

In the face of the unpredictability of human behaviors, the adoption of suitable impedance strategies to control robots in the presence of humans is an essential paradigm to ensure reliability and safety. For advanced robots, which operate in anthropic environments by cooperating with humans and substituting them in some tasks, the quality of performance is not just about accuracy and repeatability. Indeed, it rather depends on the ability of the robots to adapt their behaviors dynamically and according to the task and human intentions. In the case of redundant robots, also the redundant degrees of freedom may play an important role both in the stability of the coupled system and in the quality of performance.

To this purpose, UNINA has carried out an experimental study on a variable impedance control of a redundant manipulator not specifically designed for human-robot cooperation, used for the execution of a task under human guidance. In particular, a cooperative writing task is used as case study and a Cartesian impedance control law is adopted to achieve a compliant behavior of the end effector with respect to the forces exerted by the human operator. This approach is described in the first part of this report (Sec. 2).

The approach pursued is that of using in a synergic way the robot's redundancy and the modulation of the Cartesian impedance parameters to enhance the performance during human-robot physical interaction. In particular, an experimental evaluation of different impedance modulation laws within a stability region is carried out, while it is shown that the overall performance can be improved when the redundancy is used to enlarge the stability region in the space of the impedance parameters.

The experimental results show that the variable impedance control performs better than the impedance control with constant parameters, in the sense that it preserves accuracy while reducing the execution time, in comparison to high constant impedance, and it guarantees a good execution speed with increased accuracy, in comparison to low constant impedance. Finally, the use of the variable impedance strategy together with Cartesian inertia decoupling through redundancy resolution is the combination that allows the best performance and effectively enhances the comfort level perceived by the human operators during manual guidance.

The idea of attaching the robot link to the motor via elastic elements is especially motivated by the possibility to store potential energy in the springs, which enables movement types that could not be implemented with rigid joints. Nevertheless, the additional (adjustable) elasticity makes VSA robots also more difficult to control as the torques acting on the link side depend now on the deflection of the corresponding elastic elements meaning that motor torques only indirectly influence the movement of these robots.

DLR followed several approaches for solving this control problem and designed controllers which make explicit use of the (adjustable) elasticity of VSA robots to perform efficient movements that are suited for interacting with humans. The latter part of this report will summarize these approaches (Sec. 3). The experimental results, which were obtained following these approaches, will be presented in Deliverable D3.2.2 (at month 48).

2 Variable Impedance Control

The control strategy is designed to perform tasks in cooperation with humans. The operator interacts with the robot by moving the end effector along arbitrary trajectories. It is assumed that only forces can be applied.

The dynamic model of a rigid manipulator interacting with the (human) environment is given by

$$\boldsymbol{M}(\boldsymbol{q})\ddot{\boldsymbol{q}} + \boldsymbol{C}(\boldsymbol{q},\dot{\boldsymbol{q}})\dot{\boldsymbol{q}} + \boldsymbol{g}(\boldsymbol{q}) + \boldsymbol{\tau}_f = \boldsymbol{\tau}_c + \boldsymbol{J}^T(\boldsymbol{q})\boldsymbol{F}_{ext}, \tag{1}$$

with positive definite inertia matrix $\boldsymbol{M}$, Coriolis and centrifugal velocity terms $\boldsymbol{C}\dot{\boldsymbol{q}}$ (factorized by the Christtoffel symbols), gravitational terms $\boldsymbol{g}$, friction torques $\boldsymbol{\tau}_f$, control torque $\boldsymbol{\tau}_c \in \mathbb{R}^n$, and joint torque $\boldsymbol{J}^T(\boldsymbol{q})\boldsymbol{F}_{ext}$ resulting from the contact interaction force $\boldsymbol{F}_{ext} \in \mathbb{R}^3$.

To design the impedance control, it is useful to derive the end effector dynamics in the operational space [4], considering only the translational motion:

$$\boldsymbol{\Lambda}(\boldsymbol{q})\ddot{\boldsymbol{x}} + \boldsymbol{\mu}(\boldsymbol{q},\dot{\boldsymbol{q}})\dot{\boldsymbol{x}} + \boldsymbol{F}_g(\boldsymbol{q}) + \boldsymbol{F}_f(\boldsymbol{q}) = \boldsymbol{F}_c + \boldsymbol{F}_{ext} \tag{2}$$

where $\boldsymbol{x} \in \mathbb{R}^3$ is the Cartesian position vector of the end effector, $\boldsymbol{\Lambda} = (\boldsymbol{J}\boldsymbol{M}^{-1}\boldsymbol{J}^T)^{-1}$ is the (3×3) end effector inertia matrix, hereafter denoted as apparent inertia, while $\boldsymbol{\mu}\dot{\boldsymbol{x}} = \boldsymbol{\Lambda}(\boldsymbol{J}\boldsymbol{M}^{-1}\boldsymbol{C} - \dot{\boldsymbol{J}})\dot{\boldsymbol{q}}$, $\boldsymbol{F}_g = \boldsymbol{J}^{\dagger T}\boldsymbol{g}$, $\boldsymbol{F}_f = \boldsymbol{J}^{\dagger T}\boldsymbol{\tau}_f$ and $\boldsymbol{F}_c = \boldsymbol{J}^{\dagger T}\boldsymbol{\tau}_c$ are the forces, reflected at the end effector, corresponding to the non-inertial joint torques in (1).

In order to make the end effector able to follow and adapt to the force exerted by the operator at the tip, the end effector dynamics can be set as a mass-damper system of equation

$$\boldsymbol{\Lambda}_d\ddot{\boldsymbol{x}} + \boldsymbol{D}_d\dot{\boldsymbol{x}} = \boldsymbol{F}_{ext}, \tag{3}$$

where $\boldsymbol{\Lambda}_d$ and $\boldsymbol{D}_d$ are suitable inertia and damping matrices, that are positive definite and are usually set as constant diagonal matrices. The above dynamics can be imposed to the closed loop controlled system by choosing $\boldsymbol{F}_c$ in (2) as follows:

$$\boldsymbol{F}_c = \boldsymbol{\eta}(\boldsymbol{q},\dot{\boldsymbol{q}}) - \boldsymbol{\Lambda}(\boldsymbol{q})\boldsymbol{\Lambda}_d^{-1}\boldsymbol{D}_d\dot{\boldsymbol{x}} + (\boldsymbol{\Lambda}(\boldsymbol{q})\boldsymbol{\Lambda}_d^{-1} - \boldsymbol{I})\boldsymbol{F}_{ext}, \tag{4}$$

with $\boldsymbol{\eta}(\boldsymbol{q},\dot{\boldsymbol{q}}) = \boldsymbol{\mu}(\boldsymbol{q},\dot{\boldsymbol{q}})\dot{\boldsymbol{x}} + \boldsymbol{F}_g(\boldsymbol{q}) + \boldsymbol{F}_f(\boldsymbol{q})$. This equation is a Cartesian impedance control law with null stiffness and null virtual position. Force feedback is required if inertia reshaping is desired. This is the price to pay to achieve the ideal behaviour described by Eq. (3), which is linear, decoupled and independent of the robot configuration.

The external force $\boldsymbol{F}_{ext}$ can be measured by using a force/torque sensor mounted at the end effector. Alternatively, force estimation techniques can be adopted.

In view of the above approximations, the control law that imposes the impedance dynamics (3) can be implemented in the joint space in the form:

$$\boldsymbol{\tau}_{imp} = -\boldsymbol{J}^T\boldsymbol{\Lambda}[\dot{\boldsymbol{J}}\dot{\boldsymbol{q}} + \boldsymbol{\Lambda}_d^{-1}(\boldsymbol{D}_d\dot{\boldsymbol{x}} - \widehat{\boldsymbol{F}}_{ext})] + \boldsymbol{g}(\boldsymbol{q}) - \boldsymbol{J}^T\widehat{\boldsymbol{F}}_{ext}). \tag{5}$$

2.1 Redundancy resolution

In the presence of redundant degrees of freedom, which is the case considered here, it is possible to assign a secondary task in the null space of the end effector task, by using the control law:

$$\boldsymbol{\tau}_c = \boldsymbol{\tau}_{imp} + (\boldsymbol{I} - \boldsymbol{J}^T\boldsymbol{J}^{\dagger T})(\boldsymbol{u} - k_D\dot{\boldsymbol{q}}), \tag{6}$$

where $-k_D\dot{\boldsymbol{q}}$, with $k_D > 0$, is a suitable damping torque and $\boldsymbol{u}$ is a torque control input to be designed, corresponding to a secondary task, which is projected in the null space of the main task through the matrix $\boldsymbol{I} - \boldsymbol{J}^T\boldsymbol{J}^{\dagger T}$.

The preliminary results in [1] are extended through an extensive experimental study to establish the most advantageous solution for the use of redundancy. In detail, it is shown that robot's redundancy, when used to ensure a decoupled apparent inertia at the end effector, allows enlarging the stability region in the impedance parameters space and improves the performance.

Different criteria can be pursued in order to choose the secondary task.

One simple criterion can be that of keeping the robot as far as possible from kinematic singularities. This can be achieved, e.g., by maximising the kinematic manipulability index, defined as $m(\boldsymbol{q}) = \sqrt{\det(\boldsymbol{J}\boldsymbol{J}^T)}$, by choosing $\boldsymbol{u}$ in (6) as $\boldsymbol{u} = k_m\left(\frac{\partial m(\boldsymbol{q})}{\partial \boldsymbol{q}}\right)^T$.

Another possibility of exploiting redundancy is that of trying to optimise in some way the mapping between the forces applied to the end effector and the corresponding velocities or accelerations. As a matter of fact, in ideal conditions, the Cartesian impedance control law (4) allows cancelling out the robot dynamics as well as making the end effector dynamics completely independent of the joint configuration. On the other hand, it has been proven both theoretically and experimentally that, during interaction, instability is likely to occur when the controller attempts to impose to the robot a dynamic behaviour that differs significantly from the intrinsic hardware dynamics (in particular, lower than the natural robot impedance). Hence, the idea pursued here is that of using redundancy to make the robot apparent dynamics at the end effector, described by (2), as close as possible to the desired dynamics (3).

As in [1], this is achieved by using a secondary task function inspired to the dynamic conditioning index (DCI) introduced in [5] to measure the dynamic isotropy of robot manipulators in joint space.

In the Cartesian space, the DC index can be defined as the least-squares difference between the generalised inertia matrix and a diagonal matrix as $\omega(\boldsymbol{q}) = \frac{1}{2}\boldsymbol{E}^T(\boldsymbol{q})\boldsymbol{W}\boldsymbol{E}(\boldsymbol{q})$, where $\boldsymbol{W}$ is a diagonal weighting matrix and the error vector is $\boldsymbol{E}(\boldsymbol{q})^T = \left[\lambda_{11}(\boldsymbol{q}) - \sigma(\boldsymbol{q}), \lambda_{22}(\boldsymbol{q}) - \sigma(\boldsymbol{q}), \lambda_{33}(\boldsymbol{q}) - \sigma(\boldsymbol{q}), \lambda_{12}(\boldsymbol{q}), \lambda_{13}(\boldsymbol{q}), \lambda_{23}(\boldsymbol{q})\right]$, being λ_{ij} the generic element of the inertia matrix $\boldsymbol{\Lambda}$ and σ defined as $\sigma(\boldsymbol{q}) = \frac{1}{3}\text{trace}(\boldsymbol{\Lambda}(\mathbf{q}))$. The minimisation of $\omega(\boldsymbol{q})$ results in a minimisation of the elements' norm of $\boldsymbol{E}$, which corresponds to (a local) maximally diagonal inertia.

The weighting matrix $\boldsymbol{W}$ has been chosen in order to give priority to the minimisation of the norm of the off-diagonal elements of $\boldsymbol{\Lambda}(\boldsymbol{q})$, e.g. $\boldsymbol{W} = \text{diag}\{\boldsymbol{I}_3, \mu\boldsymbol{I}_3\}$ with $\mu > 1$ and $\boldsymbol{I}_3$ denoting the (3×3) identity matrix.

Finally, the control input $\boldsymbol{u}$ to assign the secondary task is chosen as $\boldsymbol{u} = -k_c \left(\frac{\partial\omega(\boldsymbol{q})}{\partial\boldsymbol{q}}\right)^T$, with $k_c > 0$.

2.2 Stability region

The stability region in the impedance parameters space could be estimated analytically (see, e.g., [3]). However, many authors have observed that the actual bounds of the stability region are dependent on the robot's hardware and, in the case of interaction with a human operator, also on the impedance of the human arm, which cannot be accurately modelled and evaluated. A further complication here is represented by the null-space stability for the presence of redundant degrees of freedom. Therefore, in this work the stability region has been found experimentally.

A suitable procedure has been set up to find the allowed range of variation of the impedance parameters of (3) so that stability is preserved, for more detailes see [2].

The results of the experimental procedure are reported in Fig. 1, where the stability region for the parameters D and α,scaling factor of the inertia matrix, is that included between the continuous and the dotted line.

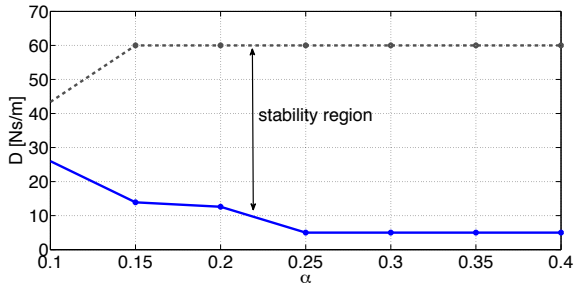

Figure 1: Range of minimum and maximum allowed damping D for a given scaling factor α of the inertia matrix.

2.3 Variable impedance

The goal of a variable impedance strategy for a co-manipulation task is to vary the damping and mass properties of the robot in order to accommodate the human movement during physical interaction. High impedance parameters are desired when the operator performs fine movements at low velocity while lower values of the parameters should be used for large movements at high velocity. The human perception is mainly influenced by the damping parameter, while, for a given damping, the desired (virtual) mass is crucial for stability.

Therefore, the idea is that of varying the damping according to the absolute value of the end effector Cartesian velocity in order to improve the performance in terms of execution time and accuracy. Namely, when the velocity is high, the damping force is reduced, so that the operator can move the end effector with minimum effort and the execution time can be reduced; vice versa, at low velocity, the damping force is increased to improve accuracy. On the other hand, the virtual mass is set so as the parameters of the system remain in the stability region. To this purpose, the stability region in the parameter space has been evaluated experimentally (see Sec. 2.2) for any damping in the interval $[5, 60]$ Ns/m.

The relationships used to vary the damping for each of the Cartesian principal directions is

$$D(\dot{x}) = \min\{a\, \mathrm{e}^{-b|\dot{x}|}, 5\}. \tag{7}$$

with $a = 60$ and $b = 4$. These parameters have been chosen in order to have a variation of the damping within the interval $[5, 60]$ Ns/m for the possible range of velocities in the considered task. A saturation to the minimum value of 5 Ns/m is introduced in case of high velocity.

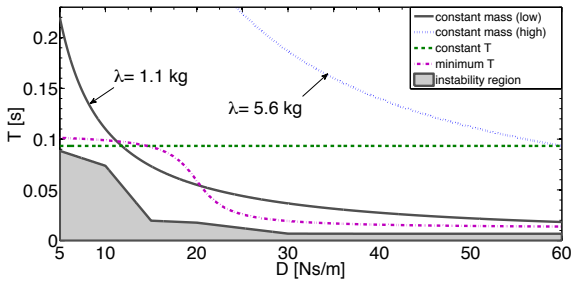

Figure 2: Representation of the four variation laws of time constant T with respect to damping D.

For the mass (or, equivalently, for the time constant T), different choices have been considered and tested, namely:

L1: constant mass, with low value (close to the minimum value within the stability region), i.e. $\lambda = 1.1$ kg

L2: constant mass, with high value, i.e. $\lambda = 5.6$ kg

L3: constant T, set as the minimum value within the stability region for any damping D

L4: minimum (variable) T within the stability region for any damping D, i.e. $T = \frac{\lambda_f}{D_f}(a + b \arctan(c(D - d)))$,

In the latter case, the default damping value $D_f = 30$ Ns/m has been chosen as an intermediate value between the minimum (5 Ns/m) and the maximum (60 Ns/m) values used in the experiments. The default mass value $\lambda_f = 3$ kg and the constant values $a = 1.1820$, $b = 0.60$, $c = 0.4$, $d = 20$ have been set in order to have the minimum allowed T preserving stability.

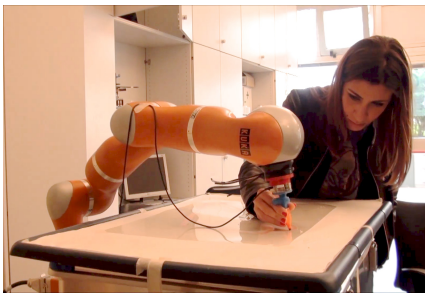

Figure 3: Snapshot of the co-manipulation task.

2.4 Experiments

In the experiments, two fundamental aspects have been considered, namely, the use of redundancy and the choice of the variable impedance strategy.

A case study has been selected, consisting in the execution of a writing task on a horizontal plane operated by a human: the operator guides a paint marker mounted on the robot's tip along a path drawn on a paper sheet.

It can be observed that, for the impedance control with constant parameters, the use of DC index (DCI) ensures better performance than the use of manipulability index (Man) both in terms of execution time and error on the path. This is true also for variable impedance control even though the use of variable parameters reduces the error on the path in spite of the strategy used to solve the redundancy.

Last but not least, all the subjects involved in the experiments have confirmed that the "feeling" of the manual guidance (in terms of intuitiveness and response of the robot) improves when the DC index is adopted, i.e., when redundancy is used to decouple the natural end effector dynamics along the principal directions of the task. For further details see [2]

Variable vs. constant impedance

The performance of the different variable impedance laws, presented in Sec. 2.3, is evaluated. The results, reported in [2] show that the lower error along the path with the smaller execution time is achieved when the virtual mass of the end effector is kept constant, to the minimum value compatible with stability, namely, the law L1 (see also Fig. 2). The variable impedance control L1 has been compared with two different sets of constant impedance gains (chosen along the curve), namely: high damping ($\lambda = 1.1$ kg, $D = 60$ Ns/m) and low damping ($\lambda = 1.1$ kg, $D = 20$ Ns/m). These values correspond to the average maximum and minimum damping recorded in the previous set of experiments with constant mass and variable damping.

The aim of this test is that of evaluating what is resulted as the best variable impedance control law for the considered task, with two different choices of constant damping values: high damping (to privilege accuracy) and low damping (to privilege execution speed).

The results, carried out on five different subjects, are shown in Fig. 4, where the execution time H and the error on the length of the path are reported. In order to assess whether the difference between the mean values on the set of data reported in Fig. 4 is statistically significant, a t-test has been performed. The results, reported in Table 1, can be interpreted as follows. If the variable h is 1 (0), than the two compared means are (not) significantly different with confidence $p \in [0, 1]$; the lower the value of p, the more statistically significant the difference between the mean values of the two sets of data. Moreover, Fig. 5 represents the norm of the linear forces exerted at the tip, for one subject, in the case of high, low and variable impedance. The horizontal dashed lines are the corresponding mean values computed during the execution of the task.

Looking at Table 1, the constant impedance with high damping (hconst) ensures higher accuracy with re-

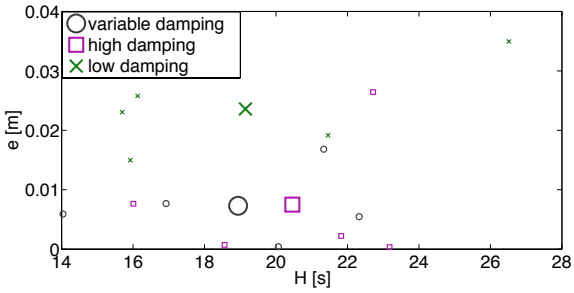

Figure 4: Values of length error e and execution time H in the experiments on five subjects using DCI optimisation, with the variable impedance control L1 and two different sets of constant parameters. The bigger markers are the mean values on the five different subjects.

Table 1: t-test results on the data of Fig. 4

	var vr hconst	var vr lconst	hconst vr lconst
time	h=1 var<hconst (p= 0.0062)	h=0 – (p= 0.8888)	h=0 – (p= 0.4503)
length	h=0 – (p=0.9739)	h=1 var<lconst (p=0.0094)	h=1 hconst<lconst (p=0.0313)

spect to the constant impedance with low damping (lconst), as expected. This result, however, comes at the expenses of the execution time and of the operator effort requested for the manual guidance. Indeed, from Fig. 5 it can be verified that higher damping requires higher forces to be exerted to the end effector. On the contrary, impedance with low damping allows the task to be performed more easily, with less effort and time, but with less accuracy.

The most relevant result of Table 1 is that the variable impedance (var) guarantees the best performance for accuracy, execution time and effort of the operator (see also Fig. 4 and Fig. 5). Indeed, it can be seen that the improvement of variable impedance (var) with respect to high constant damping (hconst) in terms of execution time is statistically significant; on the contrary it is not possible to detect an edge over the accuracy. From the comparison between the low constant damping (lconst) and variable impedance parameters (var) it emerges that the advantage of the variable strategy is relevant and statistically significant in terms of accuracy, while the difference in terms of execution time is irrelevant.

For the sake of completeness, the results of the comparison between high and low constant damping parameters have also been reported. By observing Fig. 4 and Table 1, the advantage of using high damping parameters for accuracy appears clear and statistically significant. The execution time improves when low damping is adopted since the robot become lighter and easier to move. However, the result on the execution time is not statistically significant: this is probably because the subjects were instructed to prefer accuracy over speed during the execution of the task, which has led to a higher dispersion of the data related to execution time.

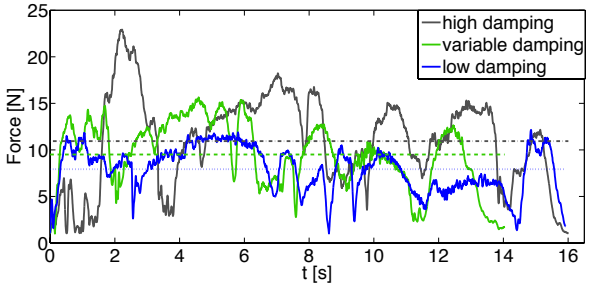

Figure 5: Norm and mean value of the contact forces for high, variable and low damping, for one subject.

3 Control Strategies for VSA Robots

In the second part of this report the dynamics of a VSA robot is taken into account

$$\boldsymbol{M}(\boldsymbol{q})\ddot{\boldsymbol{q}} + \boldsymbol{C}(\boldsymbol{q},\dot{\boldsymbol{q}})\dot{\boldsymbol{q}} + \boldsymbol{g}(\boldsymbol{q}) = \boldsymbol{\tau_J}(\boldsymbol{\varphi}) \quad (8)$$

$$\boldsymbol{B}\ddot{\boldsymbol{\theta}} + \boldsymbol{\tau_J}(\boldsymbol{\varphi}) = \boldsymbol{u}, \quad (9)$$

where $\boldsymbol{\theta} \in \mathbb{R}^n$ and $\boldsymbol{q} \in \mathbb{R}^n$ stand for the motor and link positions, respectively ($n \geq 1$). Furthermore, the motor torque is denoted by $\boldsymbol{u}$ while $\boldsymbol{M}$ and $\boldsymbol{B}$ denote the positive definite mass matrices of the robot and the motors, $\boldsymbol{C}$ the Coriolis matrix, $\boldsymbol{g}(\boldsymbol{q})$ the gravity torque vector, and finally $\boldsymbol{\varphi}$ the deflections of the springs that connect the motors to the links. The differential equations (8)-(9), which describe the motions of the motors and links, clearly show how these are coupled by the torques in these springs $\boldsymbol{\tau_J}(\boldsymbol{\varphi})$ and thus the deflections.

3.1 Regulation of energy

The first proposed control law allows to regulate the energy stored in the system to a desired value. The main idea is to first introduce an energy-like function H which is defined as the difference between the system's total energy and the potential energy the system would have at its equilibrium position given the current motor positions [6]:

$$H(\boldsymbol{\theta},\boldsymbol{q},\dot{\boldsymbol{\theta}},\dot{\boldsymbol{q}}) = \frac{1}{2}\dot{\boldsymbol{q}}^T\boldsymbol{M}\dot{\boldsymbol{q}} + U(\boldsymbol{\theta},\boldsymbol{q}) - U(\boldsymbol{\theta},\bar{\boldsymbol{q}}(\boldsymbol{\theta})), \quad (10)$$

where $\bar{\boldsymbol{q}}(\boldsymbol{\theta})$ computes the link positions of the VSA robot at the equilibrium as a function of the motor position $\boldsymbol{\theta}$. The second step is then to close the loop in (8)-(9) by the control:

$$\boldsymbol{u} = \boldsymbol{\tau}(\boldsymbol{\varphi}) - K_H\tilde{H}\left(\tau(\boldsymbol{\varphi}) - \boldsymbol{g}(\bar{\boldsymbol{q}}(\boldsymbol{\theta}))\right) - \boldsymbol{K_\theta}\tilde{\boldsymbol{\theta}} - \boldsymbol{D_\theta}\dot{\boldsymbol{\theta}}, \quad (11)$$

with $\tilde{H} = H(\boldsymbol{\theta},\boldsymbol{q},\dot{\boldsymbol{\theta}},\dot{\boldsymbol{q}}) - H_d$ and $\tilde{\boldsymbol{\theta}} = \boldsymbol{\theta} - \boldsymbol{\theta}_d$. Here, H_d denotes the desired constant value for the energy difference H and similarly $\boldsymbol{\theta}_d \in \mathbb{R}^n$ the desired constant motor positions. The constant matrices $\boldsymbol{K_\theta}$ and $\boldsymbol{D_\theta}$ and the scalar K_H are design parameters.

The control law in (11) can be mainly used for two different tasks. The first task is to drive the robot to a desired equilibrium position $\bar{\boldsymbol{q}}_d$ by setting the desired energy difference to zero ($H_d = 0$) and the desired motor positions to $\boldsymbol{\theta}_d = \bar{\boldsymbol{q}}^{-1}(\bar{\boldsymbol{q}}_d)$ (with $\bar{\boldsymbol{q}}^{-1}$ denoting the (well-defined) inverse of the function $\bar{\boldsymbol{q}}$). This equilibrium position can be shown to be an asymptotically stable equilibrium point of the closed-loop system regardless of the system's dimension n.

The second task which can be achieved using the control (11) is to excite the system in such a way that it moves on an asymptotically stable limit cycle where the motor positions are fixed meaning that on the limit cycle the whole motion is realized by the potential energy stored in the elastic elements. This in turn also implies the desired energy efficiency of the controller law. These properties of the limit cycle are, however,

for now only shown to hold for one-dimensional systems ($n = 1$). Currently, we are working on extending the results on higher dimensions.

3.2 Link-side damping using a passivity-based approach

Our second proposed control law implements a damping term for the link side dynamics given in (8) in order to regulate the robot to a desired configuration. This is achieved by introducing a new coordinate "$\boldsymbol{x}$" reflecting this damping term and shaping the dynamics of the motor such that it structurally equals the dynamics in the original coordinates. In particular, by exclusively adding a damping term to the original plant dynamics (8) we get

$$\boldsymbol{M}(\boldsymbol{q})\ddot{\boldsymbol{q}} + \boldsymbol{C}(\boldsymbol{q}, \dot{\boldsymbol{q}})\dot{\boldsymbol{q}} + \boldsymbol{g}(\boldsymbol{q}) = \boldsymbol{\tau_J}(\boldsymbol{x} - \boldsymbol{q}) - \boldsymbol{D}\dot{\boldsymbol{q}}, \tag{12}$$

where $\boldsymbol{D}$ represents a symmetric and positive definite damping matrix which is the design parameter of the proposed controller. The new coordinate $\boldsymbol{x}$ depends according to (8)-(9) and (12) on the force caused by this damping matrix as well as the forces in the system's elastic elements and the robot's current position:

$$\boldsymbol{x} = \boldsymbol{\tau_J}^{-1}(\boldsymbol{\tau_J}(\boldsymbol{\varphi}) + \boldsymbol{D}\dot{\boldsymbol{q}}) + \boldsymbol{q}, \tag{13}$$

with $\boldsymbol{\tau_J}^{-1}$ denoting the inverse function of $\boldsymbol{\tau_J}$. By feedback linearizing the motor dynamics, it is possible to find for a given torque profile $\boldsymbol{\tau_J}(\boldsymbol{\varphi})$ a well-defined transformation $\bar{\boldsymbol{u}} = \bar{\boldsymbol{u}}(\boldsymbol{u}, \boldsymbol{\theta}, \boldsymbol{q}, \boldsymbol{B})$ such that the dynamics of this new coordinate is described by the same motor dynamics as in (9) with this new control $\bar{\boldsymbol{u}}$. Finally, by letting $\bar{\boldsymbol{u}} = -\boldsymbol{K_D}\dot{\boldsymbol{x}} - \boldsymbol{K_P}(\boldsymbol{x} - \boldsymbol{x_d})$ we get our desired closed-loop system:

$$\begin{aligned} \boldsymbol{M}(\boldsymbol{q})\ddot{\boldsymbol{q}} + [\boldsymbol{C}(\boldsymbol{q}, \dot{\boldsymbol{q}}) + \boldsymbol{D}]\,\dot{\boldsymbol{q}} + \boldsymbol{g}(\boldsymbol{q}) &= \boldsymbol{\tau_J}(\boldsymbol{x} - \boldsymbol{q}) && (14) \\ \boldsymbol{B}\ddot{\boldsymbol{x}} + \boldsymbol{K_D}\dot{\boldsymbol{x}} + \boldsymbol{K_P}(\boldsymbol{x} - \boldsymbol{x_d}) + \boldsymbol{\tau_J}(\boldsymbol{x} - \boldsymbol{q}) &= \boldsymbol{0}. && (15) \end{aligned}$$

It can be shown that the closed-loop system in (14)-(15) can be represented as an interconnection of passive subsystems which in turn can be used to show that the resulting system is asymptotically stable. As already mentioned, the controlled VSA robot moves then to the desired equilibrium position $\boldsymbol{q_d}$ determined by $\boldsymbol{x_d}$ and (13).

3.3 Optimal control of motor velocity and torque profiles for maximum performance

In order to compute control strategies of VSA robots, which exploit the elasticities in the best possible way, applying optimal control (OC) theory is another way of approaching the control problem of these robots. Many numerical results justifying the performance gain of complex VSA robots have been previously shown following this approach. Nevertheless, complex systems mostly prevent us from gaining analytical insights or fully understanding the underlying OC strategy. Our third approach to the problem is to unveil the underlying control patterns for 1-DoF joints by finding analytical solutions to the corresponding OC problems with some simplifying assumptions in order to thoroughly understand the inherent capabilities of elastic robots.

After our results on the relation between the spring's potential energy and the optimal control strategy for realising explosive motions using adjustable linear springs with a velocity-controlled motor [7], we extended these results to elastic joints with adjustable nonlinear springs [9]. In particular, we built up on the method we first introduced for analysing Variable Stiffness Actuators with fixed motor positions [8] and considered now additionally the control from the motor side.

The elastic joint model that we have been investigating consists of one link and one motor, which are attached to each other via an adjustable elastic spring and moving on a plane. The velocity of the motor is assumed to be bounded and directly controlled. Similarly, we assume that the joint torque τ_J in the spring

is bounded by two continuously differentiable functions of the angular deflection $\tau_{J,1}(\phi)$, $\tau_{J,2}(\phi)$ so that we have:

$$\tau_J(\phi, \sigma) = \frac{1}{2}\left(\tau_{J,2}(\phi) + \tau_{J,1}(\phi)\right) + \frac{\sigma}{2}\left(\tau_{J,2}(\phi) - \tau_{J,1}(\phi)\right), \tag{16}$$

where $\tau_{J,1} < \tau_{J,2}$ holds for all $\phi > 0$ and the bounded stiffness controller $\sigma \in [-1, 1]$ determines the joint-torque deflection along the system's trajectory. The differential equations in (8)-(9) simplify then to:

$$M\ddot{q} = \tau_J(\phi, u_2) \tag{17}$$

$$\dot{\theta} = u_1 \in [-u_{1max}, u_{1max}]. \tag{18}$$

Applying Pontragin's Minimum Principle, we have shown that along time-optimal trajectories of this system both controllers must switch between their min. or max. values. This means, for instance, if an elastic joint is to be stopped in case of a collision with a human in minimum time, one needs to always switch between the min. and max. values for both the motor velocity $\dot{\theta}$ and the torque profile $\tau_{J,i}(i \in 1, 2)$ of the spring. Introducing a normalized deflection that indicates the ratio of the system's potential energy to its total energy and describing the system's costates in terms of this deflection, we can also compute the switching structure of both controls and thus the time-optimal bang-bang controller maximizing the joint's performance (see [9] for details).

3.4 Protection of VSA robots based on human reflexes

Our fourth approach focuses on increasing the safety and security of VSA robots by taking the human mimetic approach one step further [10]: The actuator unit consisting of motor and spring can be controlled analogously to the human muscle and tendon, which is protected by reflex actions. Those reflex actions can be interpreted on a control level to protect the mechanical system. Among them is the stretch reflex, commonly known from the tendon jerk experiment: A tap on the tendon of the quadriceps passively stretches the muscle and special receptors, the so called muscle spindles, lead to a contraction of the same muscle. Moreover, there is the more complex nociceptive withdrawal reflex that leads to a withdrawal movement elicited by a painful stimulus. The number of activated muscles is scaled with the intensity of the stimulus and might lead to the retreat of only one limb, e.g. after tapping on a needle, up to a reaction of the whole body jumping away from the source. A third reflex is the autogenic inhibition that leads to a relaxation of the muscle threatened by overload: If a force is much too strong for a muscle golgi tendon organs induce its inhibition to protect it from harmful tear.

Those reflexes are very different, but follow common principles, which are namely: hierarchy, since they operate concurrently in a predefined order, where the central nervous system (CNS) is at the highest level and can suppress any reflex activity by conscious thought; operation on joint level and not necessarily a reaction in Cartesian space; reflex reversal, which means that the same stimulus can lead to different reactions, depending on the situation; irradiation, because the stronger a stimulus the more muscles are activated and the reaction is spread (irradiated) over the joints; the preservation of a status quo, which is e.g. stability or sanity.

The reflexes, interpreted on a control level, are a combination of PD control (stretch reflex), force/torque control (autogenic inhibition) and a fast trajectory (nociceptive withdrawal reflex). We propose in our final approach an activation strategy of the reflexes based on two inputs: The measured deflection of the spring mechanism, directly correlating to the torque since the stiffness of the spring is known, and the force input from an artificial skin. The activation is complemented with a switching strategy of the control mode that preserves the stability of the system in action. Thus, the system is PD controlled and moves away from a source of stimulus to the artificial skin that is arranged in so called reflex responsive fields, eliciting a movement of the proximal joint away from the stimulus (see Fig. 6). Two of the use cases are: (A) An evasive trajectory of the motor after impact on artificial skin to a new set-point symbolized by a red dot; (B) A switch to torque

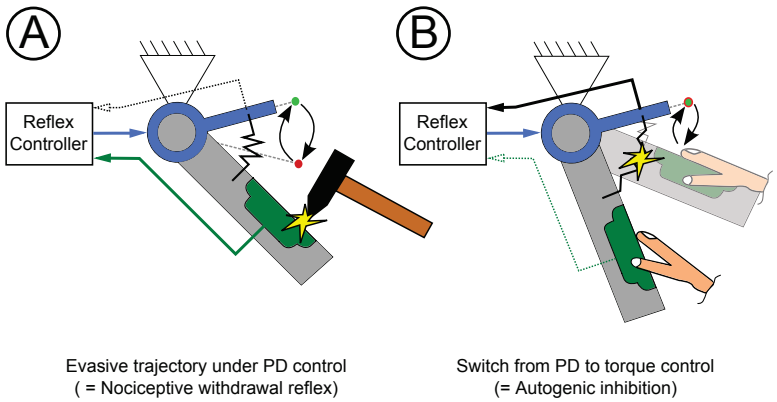

Figure 6: Control scheme for an elastic joint, where the motor is depicted in blue, the link in grey, a passive compliance as black spring and the artificial skin in green.

control mode after over-lengthening of the spring to reduce the stored elastic energy. The control modes can be used conjointly and the reaction can be spread over multiple proximal joints. After each reflexive reaction a trajectory back to original set-point, symbolized by a green dot, is computed. The stronger the stimulus, the more joints are activated to support the movement. If overload of the spring is detected, the system switches into torque control, hence reducing the energy storage in the spring, and switches back to PD control, after necessary energy and stability conditions are satisfied. All control action takes place on joint level, can be spread over multiple proximal joints as well as suppressed by raising the activation-thresholds. It only steps in when necessary and thus enhances existing control schemes by providing additional safety and security.

References

[1] F. Ficuciello, A. Romano, L. Villani, and B. Siciliano, “Cartesian impedance control of redundant manipulators for human-robot co-manipulation,” in *IEEE/RSJ Int. Conf. on Intelligent Robots and Systems*, Chicago, USA, 2014, pp. 2120–2125.

[2] F. Ficuciello, L. Villani, and B. Siciliano, “Variable Impedance Control of Redundant Manipulators for Intuitive Human-Robot Physical Interaction,” in *IEEE Transactions on Robotics*, 2015.

[3] A. Lecours, B. Mayer-St-Onge, and C. Gosselin, “Variable admittance control of a four-degree-of-freedom intelligent assist device,” in *IEEE Int. Conf. on Robotics and Automation*, Saint Paul, Minnesota, USA, 2012, pp. 3903–3908.

[4] O. Khatib, “A unified approach for motion and force control of robot manipulators: The operational space formulation,” *IEEE Journal of Robotics and Automation*, 1987, vol. 3, no. 1, pp. 1115–1120.

[5] O. Ma and J. Angeles, “The concept of dynamic isotropy and its applications to inverse kinematics and trajectory planning,” in *IEEE Int. Conf. on Robotics and Automation*, San Francisco, CA, 1990, pp. 10–15.

[6] Gianluca Garofalo, Johannes Englsberger, and Christian Ott, “On the regulation of the energy of elastic joint robots: Excitation and damping of oscillations,” In *American Control Conference (ACC), 2015*, July 2015.

[7] S. Haddadin, M. C. Özparpucu, and A. Albu-Schäffer, “Optimal control for maximizing potential energy in a variable stiffness joint,” in *Decision and Control (CDC), 2012 IEEE 51st Annual Conference on*, 2012, pages 1199–1206.

[8] M. C. Özparpucu, S. Haddadin, and A. Albu-Schäffer, “Optimal control of variable stiffness actuators with nonlinear springs,” in *Proceedings. IFAC 2014, World Congress*, 2014, pages 8487–8495.

[9] M.C. Özparpucu and A. Albu-Schäffer, “Optimal control strategies for maximizing the performance of variable stiffness joints with nonlinear springs,” in *Decision and Control (CDC), 2014 IEEE 53rd Annual Conference on*, 2014, pages 1409–1416.

[10] Sebastian Wolf, Thomas Bahls, Maxime Chalon, Werner Friedl, Markus Grebenstein, Hannes Höppner, Markus Kühne, Dominic Lakatos, Nico Mansfeld, Mehmet Can Özparpucu, Florian Petit, Jens Reinecke, Roman Weitschat, and Alin Albu-Schäffer, “Soft robotics with variable stiffness actuators: Tough robots for soft human robot interaction,” in *Soft Robotics*, 2015, pages 231–254. Springer Berlin Heidelberg.